doi: 10.3304/JMES.2018.014

Journal of Mediterranean Earth Sciences 10 (2018), 37-50

J M E S **Journal of Mediterranean Earth Sciences**

Correction factors for the effect of shape and thickness of SEM-EDS microanalysis of asbestos bundles and fibres by Monte Carlo simulation

Daniele Moro, Gianfranco Ulian and Giovanni Valdrè *

Alma Mater Studiorum - Centro di Ricerca Interdisciplinare di Biomineralogia, Cristallografia e Biomateriali, Dipartimento di Scienze Biologiche, Geologiche e Ambientali, Università di Bologna, Bologna, Italy
** Corresponding author: giovanni.valdre@unibo.it*

ABSTRACT - SEM-EDS quantitative microanalysis of asbestos mineral fibres still represents a complex analytical issue because of the variable fibre shape and small thickness (<5 μm) compared with the penetration of the incident electron beam. Size and shape of micro- and sub-micrometric particles may cause large errors in chemical quantification due to particle effects on the generation and measurement of X-rays intensity from the sample. These effects are related to the elastic scattering of electrons in the finite size (mass) of the fibre, with the scattering being strongly influenced by the average atomic number. For a given mean atomic number, the thickness of the particle is the main factor affecting X-rays intensity, with a component related to the particle shape that biases the contributions of absorption and fluorescence to the correction routine. To overcome these issues empirical methods were developed, however they are cumbersome and need characterized standards for thickness, geometry and composition. Here we present the results of Monte Carlo investigation for the thickness and shape effects on SEM-EDS and microprobe analysis of asbestos bundles. Crocidolite, amosite, tremolite-asbestos, chrysotile, anthophyllite-asbestos and actinolite-asbestos were simulated and correction factors for X-ray microanalysis were proposed. Monte Carlo simulation was used to investigate electron transport, X-ray generation and detection in asbestos bundles of variable thickness lying on a pure carbon holder. We report the results obtained on 100 μm long bundles of fibres of square section and thicknesses from to 0.1 μm to 10 μm. Realistic experimental conditions, such as sample geometry, SEM set-up and detector physics were taken into account. An electron probe of 40 nm in diameter was simulated, focussed in parallel illumination onto the surface of the bundle of fibres, in a mid position with respect to the edges. The modelled EDS detector has a resolution of 130 eV measured at Mn Kα, an elevation angle of 40°, and an azimuthal angle of 0°. The influence of thickness and shape on the simulated spectrum was investigated for electron beam energies of 5, 15 and 25 keV. A strong influence of the asbestos bundles thickness was observed. In general, the X-ray intensities as a function of bundle thickness showed a considerable reduction below about 0.5 μm at 5 keV, 2 μm at 15 keV, and 5 μm at 25 keV, with a non-linear dependence. Specific correction parameters, k-ratio, for the asbestos bundle thickness effect are here presented.

Keywords: asbestos; SEM-EDS microanalysis; Monte Carlo simulations; correction factors.

Submitted: 23 November 2017 - Accepted: 16 April 2018

1. INTRODUCTION

The term "asbestos" is used for six types of silicate mineral fibres that are or have been widely exploited in many types of technology. Asbestos belong to two mineral groups: serpentines and amphiboles. While the only asbestos of the serpentine group is chrysotile, the amphibole group contains five asbestos, i.e. crocidolite (asbestos variety of riebeckite), amosite (asbestos variety of grunerite), anthophyllite-asbestos, tremolite-asbestos and actinolite-asbestos (Hawthorne at al., 2007a; Gunter et al., 2007). The first three asbestos (chrysotile, crocidolite and amosite) are among the most employed in industrial applications. About 95% of asbestos used in commercial products was chrysotile, white asbestos (Wiewiora, 1990; Catherine and Skinner, 2003). Crocidolite, blue asbestos, and amosite, brown asbestos, are the most commonly used amphibole asbestos. They contain high levels of iron as a normal constituent of the crystal structure. Although about 95% of asbestos used in commercial products was chrysotile, amphibole exposure is greater than chrysotile in the natural environment, since amphiboles are more widespread than chrysotile (Catherine and Skinner, 2003; Gunter et al., 2007; Hawthorne and Oberti, 2007a; Hawthorne and Oberti, 2007b; Hawthorne et al., 2012). Anthophyllite-asbestos,

tremolite-asbestos and actinolite-asbestos may be found as minority phases in other fibres or in other industrially used minerals. In addition, amphiboles generally contain higher levels of iron than chrysotile. Asbestos may be found as single cylindrical fibres or as bundles of fibres, i.e. weakly bonded single fibres forming a structure with a non-cylindrical cross section. Due to the weak inter-fibres interactions, the bundles are easily separable into thinner ones. Accurate chemical analysis of asbestos mineral fibres is of paramount importance for both their identification and in depth mineral characterization. In turn, the precise knowledge of fibre composition can contribute to a deeper understanding of the impact of the mineral on health, and of the fibre characteristics that influence toxicity (Bernstein and Hoskins, 2006; Gunter et al., 2007; Bernstein, 2014).

The toxicity of asbestos fibres was demonstrated by in vitro and in vivo studies, which state that their hazardous properties can be associated to the chemical composition, and there have been suggestions that the Fe content and its oxidation state may play a role (Hardy and Aust, 1995). Furthermore, a possible genotoxic and cytotoxic mechanism could be related to the generation of reactive oxygen species and other radicals, which are catalysed by iron ions at the fibre surface (Gazzano et al., 2007). The mineralogical composition of fibres with bonded metal ions induces a strong biochemical reaction. Important contributions to biology research on the interaction between cells and fibres, that contain highly reactive chemical species, will be provided by experimental techniques able to accurately quantify the chemistry of mineral fibres in situ at both the micro- and sub-micro scale (Yao et al., 2010).

One of the most important micro-analytical technique is scanning electron microscopy equipped with X-ray energy dispersive spectroscopy (SEM-EDS), which has been successfully adopted for the characterization of minerals, materials and biomaterials, and also to evaluate the phenomena and possible mechanism of interaction between materials and bio-entities (Borgia et al., 1992; Bocchi and Valdre, 1993; Gatti et al., 1996; Valdre et al., 1999; Aparicio et al., 2009; Moro et al., 2015). Furthermore, energy dispersive X-ray spectroscopy (EDS) is by far the most routine method for asbestos chemical analysis (Gunter et al., 2007). However, particular attention must be paid with quantitative SEM-EDS microanalysis of asbestos fibres and bundles, because the variable shape of the fibre and small thickness (<5 μm) with respect to the penetration of the incident electron beam may produce systematic errors. The classical methods for the correction of matrix effects (e.g. ZAF or $\phi(\rho z)$ procedures) used in quantitative microanalysis of bulk samples assume both standard and sample to have flat polished surfaces and be infinitely thick compared to the penetration of the electron beam.

Particles with micro- and sub-micrometric sizes and shapes may cause large errors in the quantification because of particle effects on the generation and measurement of X-rays from the sample. These effects are related to the elastic scattering of electrons in the finite size (mass) of the particle, with the scattering being strongly influenced by the average atomic number. The particle size with respect to the volume of electron penetration is the main factor affecting X-rays intensity, with a component related to the particle shape that biases the contributions of absorption and fluorescence to the correction routine. X-ray absorption path length and emergence angle cannot be determined as for flat polished samples in the case of micro- and sub-micrometric particles analysis (Small, 2002; Paoletti et al., 2011). The main theme that should be clear is that EDS systems, because they are often set to normalize the results, are prone to hide poor analytical results, like high or low totals, which then hides any problem in the analytical protocol. This is commonly suspected when analysis of small samples is reported. Empirical methods were developed to overcome these problems, but they are cumbersome and need well-characterized standards for thickness, geometry and composition (Armstrong, 1991; Paoletti et al., 2008; Paoletti et al., 2011).

One effective tool to examine the issues related to the basis, the reliability and the limitations of quantification procedures is represented by the Monte Carlo method. In the context of the analysis of asbestos fibres and bundles, Monte Carlo simulations can be of paramount importance for investigating the electron transport and X-ray generation under unconventional measurement conditions or in samples with complex geometry (Salvat et al., 2006; Merlet and Llovet, 2011, 2012).

The authors recently studied electron transport and X-ray generation in chrysotile, crocidolite, amosite, anthophyllite-asbestos, tremolite-asbestos and actinolite-asbestos by means of Monte Carlo analysis, with particular attention to single fibres of cylindrical geometry (Moro and Valdrè, 2016; Valdrè et al., 2018).

In the present paper, we report the results of Monte Carlo simulations applied to the case of asbestos bundles of fibres, supposed of square section. Investigation of the effect of bundle thickness, shape and SEM chamber geometry on EDS microanalysis was performed. The Monte Carlo method was used to simulate electron transport, X-ray generation and detection in bundles of square section and to derive specific correction factors, k-ratios, for the thickness effect in the case of asbestos bundles.

2. METHODS AND SIMULATION MODELS

2.1. Methods

The Monte Carlo method allows simulating electron transport, X-ray generation, transmission, absorption and fluorescence in complex sample geometries, whose knowledge is needed to perform accurate quantitative analysis by X-ray spectroscopy. Here this approach was used to simulate electrons trajectories and X-rays generation and transmission through the asbestos

mineral bundle of fibres and to the X-ray detector.

A single scattering model is taken into account to track the trajectories of electrons as they interact with matter, together with a continuous energy loss, as reported by Ritchie (2009) and called "continuous slowing down approximation". Elastic scattering is modelled by using a basic screened Rutherford model (Myklebust et al., 1976), the Mott scattering cross section of Czyzewski and co-workers (Czyzewski et al., 1990), and the Mott cross section of Jablonski and co-workers (Jablonski et al., 2010). The energy loss is modelled using the Joy-Luo expression (Joy and Luo, 1989), which is an empirical modification of the Bethe energy loss equation (Bethe and Ashkin, 1953). The ionisation cross-section is modelled using the expression of Bote and Salvat (Bote and Salvat, 2008). The mass absorption coefficients are those of Chantler and co-workers (Chantler et al., 2005), and the fluorescence yields are tabulated experimental values (Bambynek et al., 1972).

The electron source is defined as a Gaussian beam. A response function that mimics the energy resolution of an EDS detector is convolved with the emitted X-ray events. The effects of thickness and shape were evaluated by simulating EDS spectra of asbestos bundles of fibres of square section. Peak intensities were integrated and compared as a function of thickness, shape, and beam energy for all minerals, after background subtraction. Finally, correction factors, k-ratios, for the asbestos bundle thickness effect are calculated and proposed.

2.2. Simulation models

In the present work, bundles of fibres of variable thickness placed on a pure carbon holder were simulated taking into account realistic experimental conditions, i.e. sample geometry, detector physics and SEM set-up.

The chemical formulae and mass densities of the investigated asbestos (chrysotile, crocidolite, amosite, anthophyllite-asbestos, tremolite-asbestos and actinolite-asbestos) are reported in table 1. Worth noting that there can be a range of Mg to Fe ratio within each species of amphibole, and the chemical formulae represent an average composition of the asbestos (Hawthorne et al., 2012).

For each mineral, a three-dimensional bundle model of square section deposited on a flat graphite support was considered. An example of the model geometry is reported as a 2D section in figure 1. The mineral was 100 μm long and with thicknesses ranging from 0.1 μm to 10 μm. The influence of thickness and shape on the simulated spectrum was investigated for electron beam energies of 5 keV, 15 keV and 25 keV.

An electron probe of 40 nm in diameter was considered. The probe was focussed in parallel illumination onto the surface of the bundle of fibres, in a mid position with respect to the edges. The modelled EDS detector used to generate the spectrum had an ultra-thin polymer window (Moxtek AP 3.3 film), a gold layer of 7 nm, a dead layer of 10 nm, a detector diode thickness of 3 mm, a sample-to-detector distance of 45 mm, a detector area of 10 mm^2, 4096 channels each of 10 eV and a resolution of 130 eV (FWHM at Mn Kα). The detector elevation angle was set to 40°, with an azimuthal angle of 0°. The bundle was oriented with its long axis in the same direction as the detector.

3. RESULTS AND DISCUSSION

The X-ray generation and size of the electron beam interaction volumes in conventional SEM-EDS microanalysis (employing beam energy in the range 10-30 keV) are of the order of several μm^3 in most materials. When the penetration of the primary electron beam is greater than the size of the particle, a fraction of the electron beam escapes the particle before exciting X-rays due to the finite size effect. Consequently, a portion of the electron beam scatters out of the particle volume and can excite X-rays from the adjacent particles, from the substrate or both of them. Furthermore, there is an additional effect of the beam electrons scattering outside the particle: the fact that the standard is typically a bulk material (of infinite sizes for the electron scattering) hence of much larger size and so there are more X-rays generated in the standard respect to the micro-nanosized particle or material. Thus, the k-ratio is additionally diminished because the intensity of the element X-ray in the standard (denominator of the k-ratio) is larger. Each

Mineral name	Chemical formula[a]	Mass density
Chrysotile	$Mg_3Si_2O_5(OH)_4$	2.50[b]
Crocidolite	$Na_2Fe^{2+}{}_{2.25}Mg_{0.75}Fe^{3+}{}_2Si_8O_{22}(OH)_2$	3.35[b]
Amosite	$Fe^{2+}{}_{5.25}Mg_{1.75}Si_8O_{22}(OH)_2$	3.50[b]
Anthophyllite-asbestos	$Mg_{5.25}Fe^{2+}{}_{1.75}Si_8O_{22}(OH)_2$	3.21[c]
Tremolite-asbestos	$Ca_2Mg_{4.75}Fe^{2+}{}_{0.25}Si_8O_{22}(OH)_2$	3.00[c]
Actinolite-asbestos	$Ca_2Mg_{3.5}Fe^{2+}{}_{1.5}Si_8O_{22}(OH)_2$	3.23[c]

[a] Hawthorne et al., 2012; [b] Anthony et al., 2015; [c] Haynes, 2015.

Tab. 1 - Average chemical formulae and mass density (g/cm^3) of the simulated asbestos.

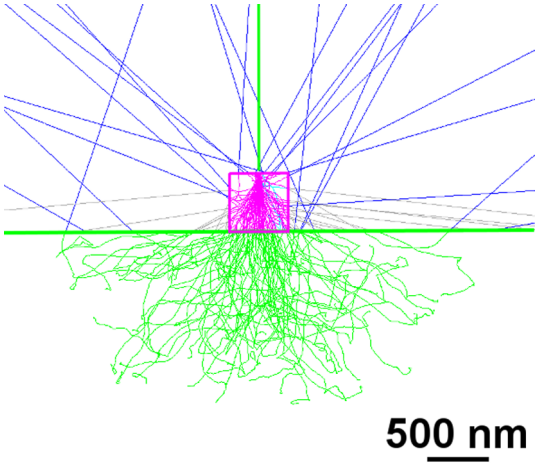

Fig. 1 - Simulated trajectory of electrons as they interact with the sample (crocidolite) and the substrate (graphite). 2D view of the 3D simulated trajectory of electrons (fuchsia: interacting with the sample; grey and green: towards and penetrating the substrate, respectively; blue: exiting) as they interact with a crocidolite bundle of fibres of square section (marked with a thick fuchsia line) deposited on a bulk graphite substrate (marked with a green horizontal line). The view is from the direction parallel to the elongation of the bundle.

described phenomena can severely affect the analytical results.

For the sake of an example, figure 1 reports the simulated trajectories of electrons for a 15 keV electron beam focussed onto the surface of a crocidolite bundle of fibres, supposed of square section, in a mid position with respect to the edges. The bundle has a thickness of 500 nm and is assumed deposited on a graphite substrate. The primary electrons (green vertical beam) interact with the mineral as visualized by the fuchsia trajectories. At this energy level (15 keV) a fraction of the electrons penetrates into the graphite substrate (green trajectories) for more than 1.5 μm, eventually exiting (blue lines). Furthermore, a fraction of the electrons scatters out of the mineral volume from its sides, both toward the substrate, grey trajectories, and leaving the mineral, blue lines.

In order to help the reader in analysing the results, some reference values for crocidolite, amosite, tremolite-asbestos, actinolite-asbestos, anthophyllite-asbestos and chrysotile bulk mineral samples, published in previous works (Moro et al., 2016, Valdrè et al., 2018), are reported in integrated form in table 2. The nominal range value of electron penetration depth and X-ray intensity (generated and emitted) for a beam energy of 15 keV are reported. The calculation was performed with the same detector physics and SEM set-up reported in Section 2.2 considering 1000 electron trajectories and a probe dose of 60 nA·s. Table 2 reports for each X-ray line the absolute magnitude of generated and emitted X-ray intensity calculated on bulk samples, in arbitrary units as reported by Ritchie (2010).

The following sections report the trends of the integrated intensities (counts) as a function of bundle thickness for crocidolite, amosite and tremolite-asbestos. The last section presents the correction factors, k-ratios, calculated for all asbestos minerals.

3.1. Crocidolite

A crocidolite bundle of fibres of square section with a composition as reported in Tab. 1 and thickness from 0.1 μm to 10 μm, deposited on a bulk graphite substrate, was simulated. The results are shown in figure 2, that reports the trend of the integrated intensities (counts), obtained from the simulated EDS spectra, as a function of bundle thickness for each element of the mineral at beam energies of 5 keV, 15 keV and 25 keV.

Generally, for all the X-ray emission lines here investigated, the simulated X-ray intensity presented a strong dependence on the bundle thickness, following a non-linear trend. It can be observed that the integrated intensity starts to have a non-linear reduction for thickness at least below 5 μm, with the exception of the Fe L line whose intensity starts decreasing below 2 μm of thickness (see Fig. 2g). Going into details, for almost all the considered X-ray emission lines, Si Kα, Mg Kα, O Kα, Na Kα, Fe Kα, Fe Kβ, Fe L, the integrated intensity strongly decreases starting from thickness of about 5 μm at 25 keV, 2 μm at 15 keV and 0.5 μm at 5 keV. The intensity values calculated for thickness of 10 μm were found very close to those calculated for a massive sample. These observation are in line with the results obtained in the case of a single fibre of cylindrical geometry (Moro and Valdrè, 2016).

The simulation shows an effect of intensity enhancement before the reduction starting point, different for each specific X-ray emission line and electron beam energy. Taking into account the previously cited finite size and reduced absorption effects, the last one initially prevails on the finite size effect, that in turn become predominant for smaller thicknesses.

As can be observed in figure 2, the magnitude of the reduced X-ray absorption effect is generally largest in the case of "soft" X-rays (O Kα, Fe L, Na Kα), for which there is high absorption, in agreement with the experimental results of both Paoletti et al. (2011) and Small (2002).

It should be noted that Fe Kα and Fe Kβ X-rays emission lines cannot be excited by a low energy beam of 5 keV (Fig. 2 e,f).

The same effect of intensity enhancement is observed for both the bundle geometry here simulated and the cylindrical fibre geometry in Moro and Valdrè (2016). However, it is generally more pronounced in the case of the cylindrical fibre geometry.

3.2. Amosite

Bundles of fibres of square section of amosite with the composition reported in Tab. 1 and thickness from 0.1 μm to 10 μm, deposited on a bulk graphite substrate, were simulated. The results are shown in figure 3, reporting the trend of the integrated intensities (counts),

	Crocidolite	Amosite	Asbestos tremolite	Asbestos actinolite	Asbestos anthophyllite	Chrysotile
e.p.d. [μm]	1.76	1.47	1.74	1.81	1.74	2.20
Na Kα	(g) 38	-	-	-	-	-
	(e) 14					
Ca Kα	-	-	(g) 87	(g) 85	-	-
			(e) 81	(e) 80		
Ca Kβ	-	-	(g) 9	(g) 9	-	-
			(e) 9	(e) 9		
Mg Kα	(g) 14	(g) 30	(g) 367	(g) 410	(g) 410	(g) 170
	(e) 7	(e) 15	(e) 230	(e) 240	(e) 240	(e) 110
(g) 410						
Fe Kα	(g) 21	(g) 24	(g) 4	(g) 26	(g) 31	-
	(e) 21	(e) 24	(e) 4	(e) 26	(e) 31	
Fe Kβ	(g) 2.6	(g) 3.0	(g) 1	(g) 3	(g) 4	-
	(e) 2.5	(e) 3.0	(e) 1	(e) 3	(e) 4	
Fe L	(g) 130	(g) 150	(g) 15	(g) 88	(g) 107	-
	(e) 30	(e) 40	(e) 3	(e) 18	(e) 23	
Si Kα	(g) 140	(g) 130	(g) 582	(g) 570	(g) 588	(g) 100
	(e) 100	(e) 90	(e) 435	(e) 424	(e) 422	(e) 70
O Kα	(g) 470	(g) 440	(g) 496	(g) 486	(g) 1503	(g) 550
	(e) 190	(e) 180	(e) 418	(e) 421	(e) 581	(e) 220

Tab. 2 - Electron penetration depth (e.p.d., in μm) and absolute magnitude (in arbitrary units) of generated (g) and emitted (e) X-ray intensity for each X-ray line calculated on bulk samples of crocidolite, amosite, asbestos tremolite, asbestos actinolite, asbestos anthophyllite and chrysotile with a beam energy of 15 keV. Fe L=Lα+Lβ+Lγ. (data from Moro and Valdrè, 2016; Valdrè et al., 2018)

obtained from the simulated EDS spectra, as a function of bundle thickness for each element of the mineral at beam energies of 5 keV, 15 keV and 25 keV.

For all the X-ray emission lines here investigated, a strong dependence of the simulated X-ray intensity on the bundle thickness was observed, with a non-linear trend specific for the amosite mineral. The integrated intensity starts reducing below a sample thickness of at least 5 μm, with the exception of the Fe L line, that starts decreasing from 2 μm (see Fig. 3f). In details, for almost all the considered X-ray emission lines, Si Kα, Mg Kα, O Kα, Fe Kα, Fe Kβ, Fe L, the integrated intensity strongly decreases starting from thickness of about 5 μm at 25 keV, 2 μm at 15 keV and 0.5 μm at 5 keV. The intensity values calculated for thickness of 10 μm were found very close to those calculated for a massive sample. These observation are in line with the results obtained in the case of a single fibre of cylindrical geometry (Moro and Valdrè, 2016). Also for amosite the simulation clearly shows an effect of intensity enhancement before the reduction starting point, different for each specific X-ray emission line and electron beam energy. Again, in terms of the previously cited finite size and reduced absorption effects, the last one initially prevails on the finite size effect, that in turn becomes predominant for smaller thicknesses.

The same effect of intensity enhancement is observed for both the bundle geometry here simulated and the cylindrical fibre geometry in Moro et al. (2016). However, it is generally more pronounced in the case of the cylindrical fibre geometry.

It should be noted that Fe Kα and Fe Kβ X-rays emission lines cannot be excited by a low energy beam of 5 keV (Fig. 3 d,e).

3.3. Asbestos Tremolite

A tremolite-asbestos bundle of fibres of square section with a composition as reported in table 1 and thickness from 0.1 μm to 10 μm, deposited on a bulk graphite substrate, was also simulated. See section 2.2 for further details on the simulation model. The results are shown in figure 4, that reports the trend of the integrated intensities (counts), obtained from the simulated EDS spectra, as a function of bundle thickness for each element of the mineral (Ca, Mg, Fe, Si, O) at beam energies of 5 keV, 15 keV and 25 keV.

Generally, for all the X-ray emission lines here investigated, the simulated X-ray intensity presented a strong dependence on the bundle thickness, following a non-linear trend. It can be observed that the integrated intensity starts to have a non-linear reduction for thickness at least below 5 μm. In particular, for almost all the considered X-ray emission lines, Ca Kα, Ca Kβ,

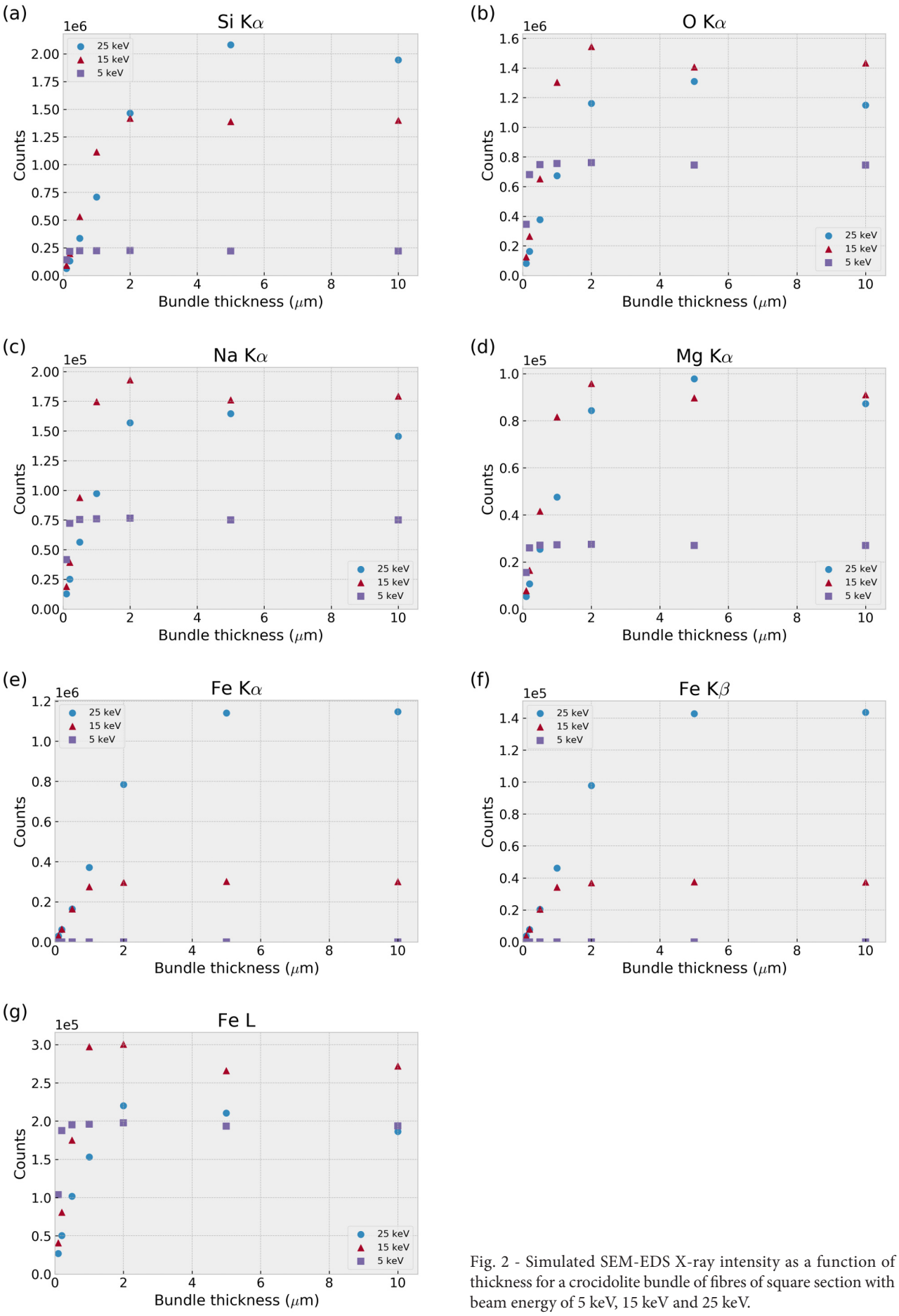

Fig. 2 - Simulated SEM-EDS X-ray intensity as a function of thickness for a crocidolite bundle of fibres of square section with beam energy of 5 keV, 15 keV and 25 keV.

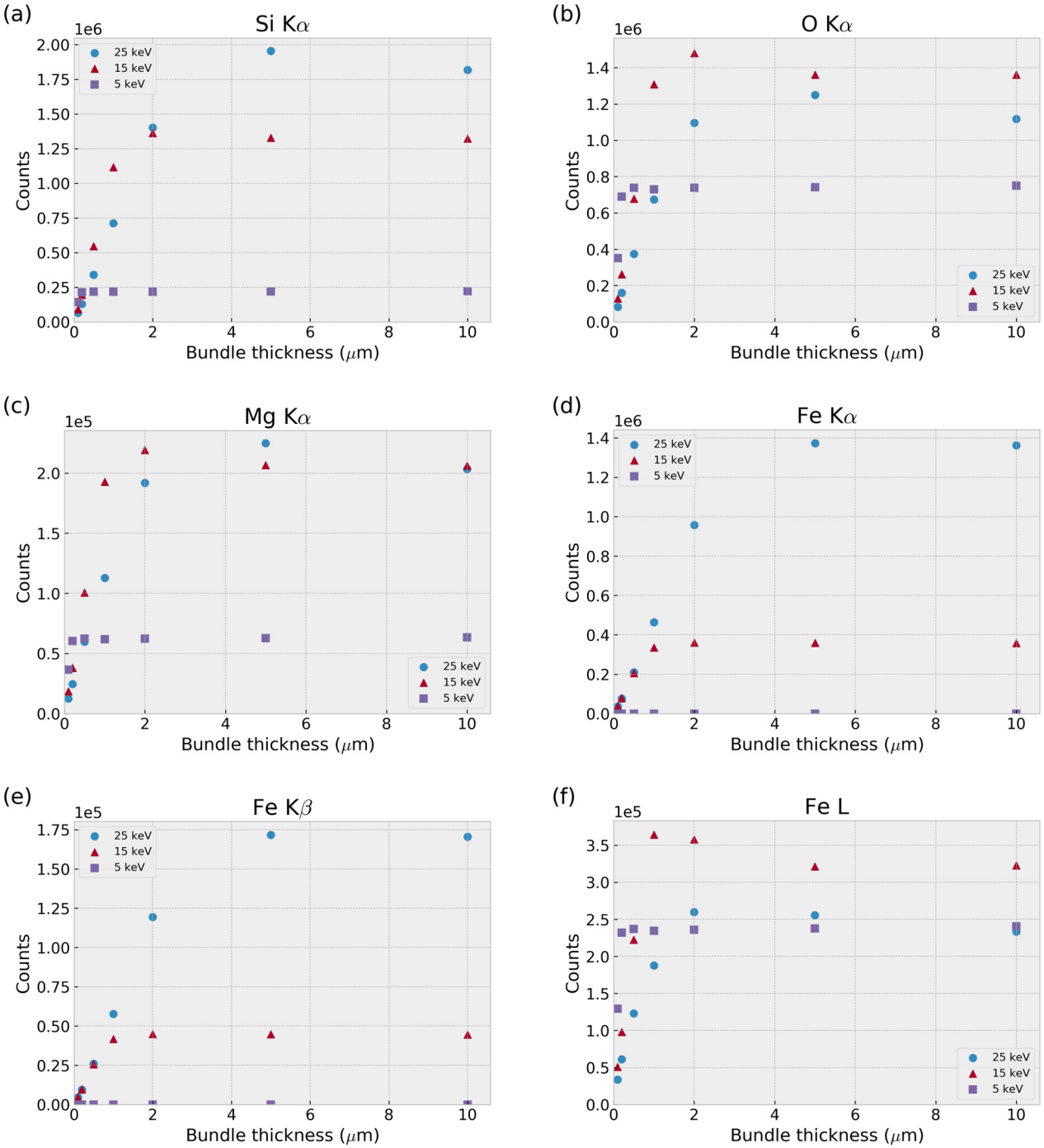

Fig. 3 - Simulated SEM-EDS X-ray intensity as a function of thickness for an amosite bundle of fibres of square section with beam energy of 5 keV, 15 keV and 25 keV.

Mg Kα, Fe Kα, Fe Kβ, Fe L, Si Kα, O Kα, the integrated intensity strongly decreases starting from thickness of about 5 μm at 25 keV, 2 μm at 15 keV and 0.5 μm at 5 keV. The intensity values calculated for thickness of 10 μm were found very close to those calculated for a massive sample. These observation are in line with the results obtained in the case of a single fibre of cylindrical geometry (Valdrè et al., 2018).

Also in the case of tremolite-asbestos an effect of intensity enhancement before the reduction starting point was observed, see figure 4. The magnitude of the reduced X-ray absorption effect is generally largest in the case of "soft" X-rays (O Kα, Fe L), for which there is high absorption, in agreement with the experimental results of both Paoletti et al. (2011) and Small (2002).

However, a less marked increase in intensity was observed in the case of tremolite-asbestos with respect to crocidolite and amosite. The same effect of intensity enhancement is observed for both tremolite-asbestos bundle geometry here simulated and the cylindrical fibre geometry in Valdrè et al. (2018). However, it is generally more pronounced in the case of the cylindrical fibre geometry.

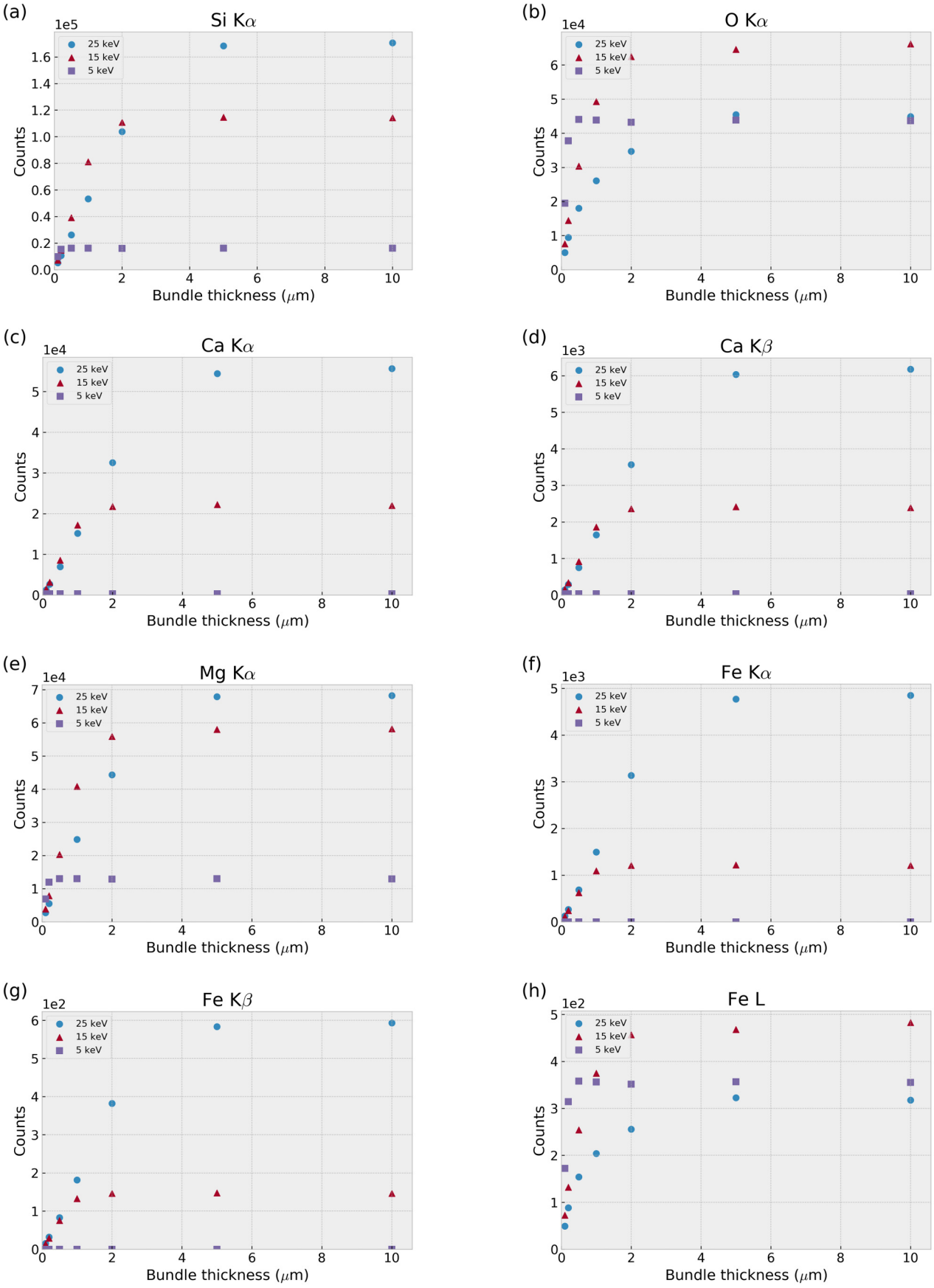

Fig. 4 - Simulated SEM-EDS X-ray intensity as a function of thickness for a tremolite-asbestos bundle of fibres of square section with beam energy of 5 keV, 15 keV and 25 keV.

It should be noted that a beam energy of 5 keV cannot excite Fe Kα and Fe Kβ X-rays (Fig. 4 f,g), and the overvoltage ratio is too low for efficient generation of Ca Kα and Ca Kβ X-rays (in this specific case just about 100 counts, difficult to be appreciated in figure 4 c,d).

3.4. Asbestos Actinolite

An asbestos actinolite bundle of fibres of square section with a composition as reported in table 1 and thickness from 0.1 μm to 10 μm, deposited on a bulk graphite substrate, was also simulated. See section 2.2 for further details on the simulation model. The results are shown in figure 5, that reports the trend of the integrated intensities (counts), obtained from the simulated EDS spectra, as a function of bundle thickness for each element of the mineral (Ca, Mg, Fe, Si, O) at beam energies of 5 keV, 15 keV and 25 keV, respectively.

Similarly to the results on tremolite-asbestos bundles of fibres, it can be observed that the integrated intensity starts to have a non-linear reduction for thickness at least below 5 μm. In particular, for almost all the considered X-ray emission lines, Ca Kα, Ca Kβ, Mg Kα, Fe Kα, Fe Kβ, Fe L, Si Kα, O Kα, the integrated intensity strongly decreases starting from thickness of about 5 μm at 25 keV, 2 μm at 15 keV and 0.5 μm at 5 keV. The trend of the integrated intensity as a function of the bundle thickness is comparable with that of tremolite-asbestos bundles, as well as the effect of intensity enhancement before the reduction starting point for O Kα and Fe L.

It should be noted that a beam energy of 5 keV cannot excite Fe Kα and Fe Kβ X-rays (Fig. 5 f,g), and the overvoltage ratio is too low for efficient generation of Ca Kα and Ca Kβ X-rays (in this specific case just about 100 counts, difficult to be appreciated in figure 5c and 5d).

3.5. Asbestos Anthophyllite

Data on bundles of fibres of square section of asbestos anthophyllite with the composition reported in table 1 and thickness from 0.1 μm to 10 μm, deposited on a bulk graphite substrate, were previously obtained (Valdrè et al., 2018) and are here discussed in comparison with those of the cylindrical fibre geometry. The results are shown in figure 6, reporting the trend of the integrated intensities (counts), obtained from the simulated EDS spectra, as a function of bundle thickness for each element of the mineral at beam energies of 5 keV, 15 keV and 25 keV, respectively.

For all the X-ray emission lines here investigated, a strong dependence of the simulated X-ray intensity on the bundle thickness was observed, with a non-linear trend similar between the bundles of fibres of square section and the cylindrical fibre geometry. In both cases, the integrated intensity starts to have the non-linear reduction for thickness at least below 5 μm. In details, for almost all the considered X-ray emission lines, Si Kα, Mg Kα, O Kα, Fe Kα, Fe Kβ, Fe L, the integrated intensity strongly decreases starting from thickness of about 5 μm at 25 keV, 2 μm at 15 keV and 0.5 μm at 5 keV. A comparable effect of intensity enhancement before the reduction starting point, different for each specific X-ray emission line and electron beam energy, is observed for the bundle and the cylindrical fibre geometry.

It should be noted that Fe Kα and Fe Kβ X-rays emission lines cannot be excited by a low energy beam of 5 keV (Fig. 6 d,e).

3.6. Chrysotile

Also in the case of chrysotile bundle of fibres of square section (data from Moro and Valdrè, 2016, here reported for a comparison) a non-linear trend of the X-ray intensity as a function of the bundle thickness was observed (Fig. 7). The integrated intensity starts to have a non-linear reduction for thickness at least below 5 μm. Again, an effect of intensity enhancement before the reduction starting point, different for each electron beam energy, is observed, larger in the case of O Kα X-rays.

3.7. Correction factors, k-ratios

The aim of the present investigation was to develop specific thickness correction parameters for SEM-EDS quantitative analysis of asbestos minerals in the case of bundles of fibres. We report in table 3 the k-ratios (intensity ratio of X-rays emitted by the asbestos mineral bundles, as a function of their thickness, to those produced by a massive sample, i.e. "infinite" thickness) calculated for bundles of square section of the six investigated asbestos (crocidolite, amosite, tremolite-asbestos, chrysotile, asbestos anthophyllite and asbestos actinolite) with thickness of 0.1 μm, 0.5 μm, 1 μm and 2 μm, in the case of an electron beam energy of 15 keV. It should be remembered that the k-ratios were calculated for data simulated in our specific experimental conditions for the mineral chemistry presented in table 1, taking into account the detector characteristics and SEM experimental set-up.

4. CONCLUSIONS

For all the asbestos mineral bundles of fibres and X-ray emission lines here investigated the calculations of detected EDS X-ray intensity revealed a strong influence of the mineral thickness and shape. It was shown that the mineral bundle thickness is the main factor affecting the variation of the simulated X-ray intensity, however with a not negligible shape component affecting the specific amount of intensity reduction. A non-linear dependence of the X-ray intensity trends as a function of thickness was observed for all the elements and minerals. In general, the X-ray intensity showed a considerable reduction for thicknesses below about 5 μm at 25 keV, 2 μm at 15 keV and 0.5 μm at 5 keV, as the excitation volume is greatly reduced by using low accelerating voltages. Furthermore, an effect of X-ray intensity enhancement (reduced absorption effect) before the X-ray intensity reduction starting point was often observed. Its magnitude depends on the mineral type, shape, specific element and beam energy, and was found to be less pronounced for the bundles of square section with respect to the single cylindrical fibres. In particular, this

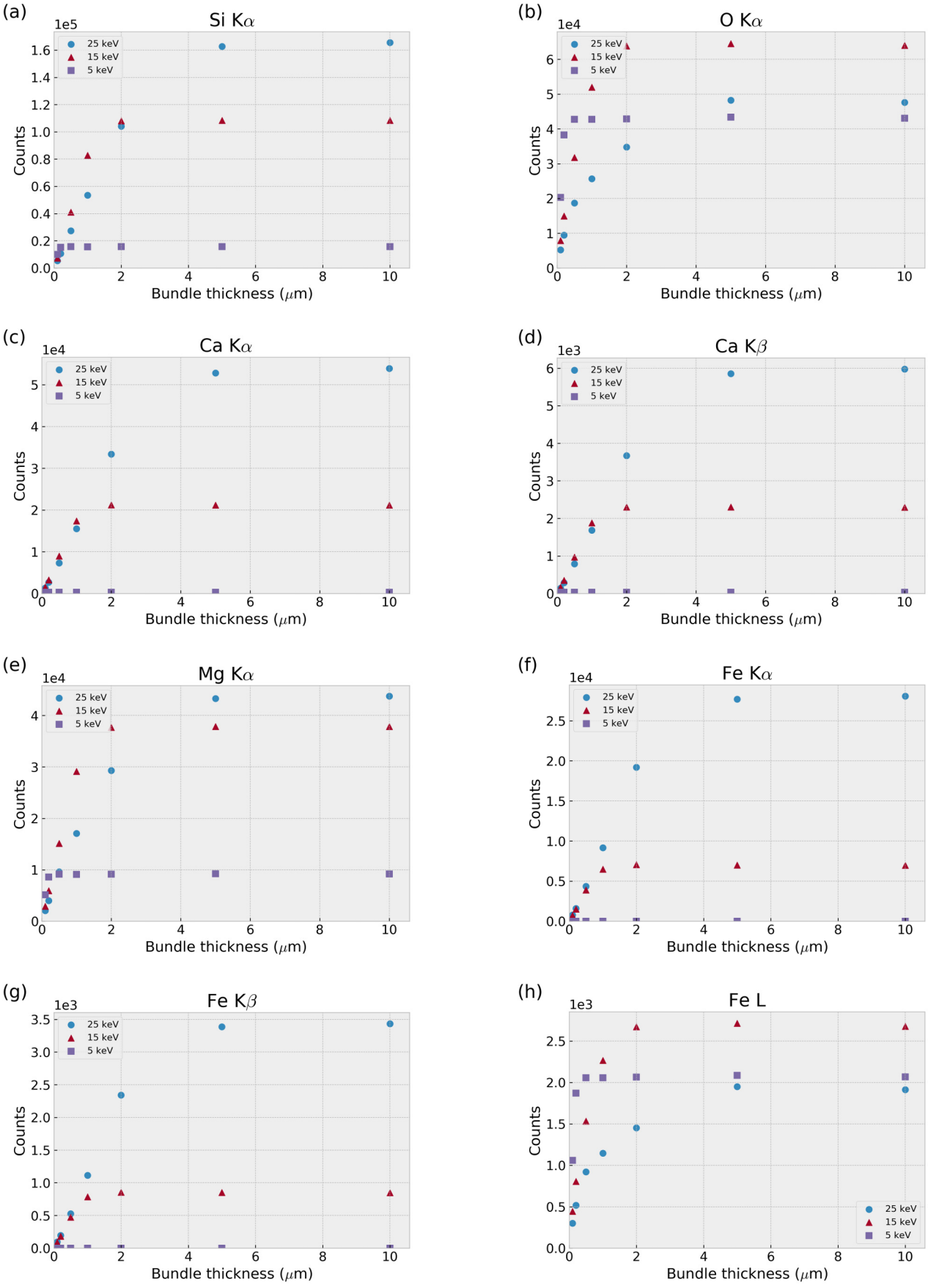

Fig. 5 - Simulated SEM-EDS X-ray intensity as a function of thickness for an actinolite-asbestos bundle of fibres of square section with beam energy of 5 keV, 15 keV and 25 keV.

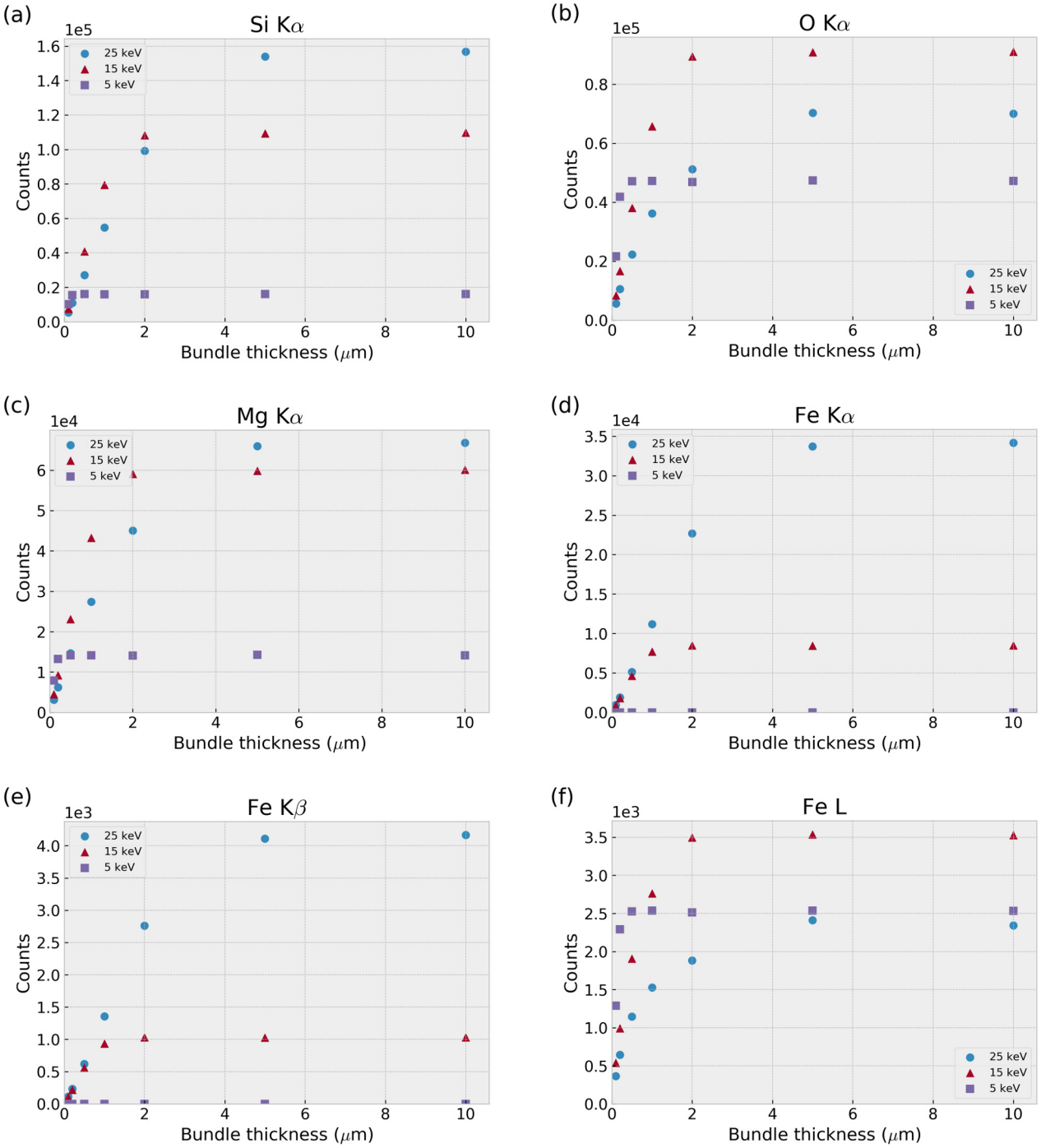

Fig. 6 - Simulated SEM-EDS X-ray intensity as a function of thickness for an anthophyllite-asbestos bundle of fibres of square section with beam energy of 5 keV, 15 keV and 25 keV. (modified from Valdre et al., 2018)

effect is enhanced for "soft" X-rays, such as for example O Kα, Na Kβ, Fe L X-ray emission lines in crocidolite, and O Kα and Fe L in amosite and tremolite-asbestos, in accordance to experimental data of both Paoletti et al. (2011) and Small (2002). A much less marked increase in intensity was observed in the case of tremolite-asbestos. The Monte Carlo simulation method has proved to be an effective tool, competitive with other complex experimental methods, allowing the calculation of correction k-ratios factors.

REFERENCES

Anthony J.W., Bideaux R.A., Bladh K.W., Nichols M.C., (Eds.), 2015. Handbook of Mineralogy. Mineralogical Society of America, Chantilly, VA, USA. http://www.handbookofmineralogy.org/.

Aparicio P., Galan E., Valdrè G., Moro D., 2009. Effect of pressure on kaolinite nanomorphology under wet and dry conditions Correlation with other kaolinite properties.

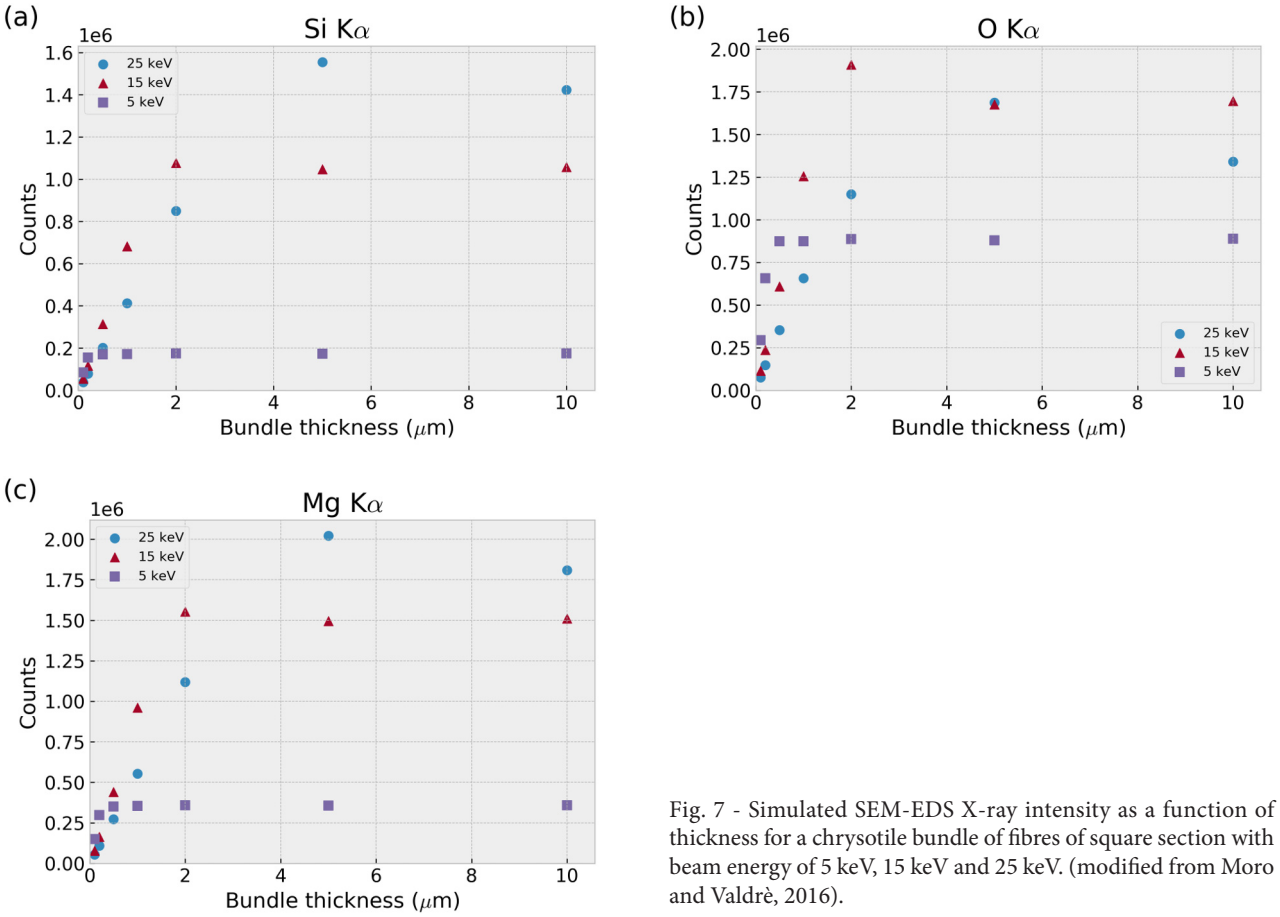

Fig. 7 - Simulated SEM-EDS X-ray intensity as a function of thickness for a chrysotile bundle of fibres of square section with beam energy of 5 keV, 15 keV and 25 keV. (modified from Moro and Valdrè, 2016).

Applied Clay Science, 46, 202-208.

Armstrong J.T., 1991. Quantitative elemental analysis of individual microparticles with electron-beam instruments. Electron Probe Quantitation. New York Plenum Press, 261-315.

Bambynek W., Crasemann B., Fink R.W., Freund H.U., Mark H., Swift C.D., Price R.E., Venugopala Rao P., 1972. X-Ray fluorescence yields, Auger, and Coster-Kronig transition probabilities Reviews of Modern Physics 44, 716-813.

Bernstein D.M., 2014. The health risk of chrysotile asbestos. Current Opinion in Pulmonary Medicine 20, 366-370.

Bernstein D.M., Hoskins J.A., 2006. The health effects of chrysotile: Current perspective based upon recent data. Regulatory Toxicology and Pharmacology, 45, 252-264.

Bethe H.A., Ashkin J., 1953. Passage of radiation through matter. In Segre E. (Ed.), Experimental Nuclear Physics, 1. John Wiley & Sons, New York, N.Y.

Bocchi G., Valdre G., 1993. Physical, chemical, and mineralogical characterization of carbonate-hydroxyapatite concretions of the human pineal-gland. Journal of Inorganic Biochemistry 49, 209-220.

Borgia G.C., Brown R.J.S., Fantazzini P., Mesini E., Valdre G., 1992. Diffusion-weighted spatial information from H-1 relaxation in restricted geometries. Nuovo Cimento della Società Italiana di Fisica D-Condensed Matter Atomic Molecular and Chemical Physics Fluids Plasmas Biophysics 14, 745-759.

Bote D. and Salvat F., 2008. Calculations of inner-shell ionization by electron impact with the distorted-wave and plane-wave born approximations. Physical Review A, 77, 042701.

Catherine H., Skinner W., 2003. Mineralogy of asbestos minerals. Indoor and Built Environment 12, 385-389.

Chantler C.T., Olsen K., Dragoset R.A., Chang J., Kishore A.R., Kotochigova S.A., Zucker D.S., 2005. NIST standard reference database version 2.1. National Institute of Standards and Technology, Available at http://physics.nist.gov/ffast.

Czyzewski Z., Maccallum D.O., Romig A., Joy D.C., 1990. Calculations of mott scattering cross-section. Journal of Applied Physics 68, 3066-3072.

Gatti A.M., Valdre G., Tombesi A., 1996. Importance of microanalysis in understanding mechanism of transformation in active glassy biomaterials. Journal of Biomedical Materials Research 31, 475-480.

Gazzano E., Turci F., Foresti E., Putzu M.G., Aldieri E., Silvagno F., Lesci I.G., Tomatis M., Riganti C., Romano C., Fubini B., Roveri N., Ghigo D., 2007. Iron-loaded synthetic chrysotile: A new model solid for studying the role of iron in asbestos toxicity. Chemical Research in Toxicology 20, 380-387.

Gunter M.E., Belluso E., Mottana A., 2007. Amphiboles: Environmental and health concerns. Amphiboles: Crystal Chemistry, Occurrence, and Health Issues 67, 453-516.

Hardy J.A. and Aust A.E., 1995. Iron in asbestos chemistry and carcinogenicity. Chemical Reviews 95, 97-118.

Hawthorne F.C., Oberti R., 2007a. Classification of the amphiboles. Amphiboles: Crystal Chemistry, Occurrence,

Mineral	Thickness	X-ray lines								
		Na_{Ka}	Ca_{Ka}	Ca_{Kb}	Fe_{Ka}	Fe_{Kb}	Fe_{L}	Mg_{Ka}	Si_{Ka}	O_{Ka}
Crocidolite	2.0 mm	1.07	-	-	0.99	0.99	1.09	1.05	1.01	1.08
	1.0 mm	0.97	-	-	0.91	0.91	1.08	0.90	0.80	0.91
	0.5 mm	0.52	-	-	0.55	0.55	0.64	0.46	0.38	0.45
	0.1 mm	0.11	-	-	0.10	0.10	0.15	0.09	0.07	0.09
Amosite	2.0 mm	-	-	-	1.01	1.01	1.12	1.07	1.03	1.10
	1.0 mm	-	-	-	0.94	0.94	1.14	0.94	0.85	0.97
	0.5 mm	-	-	-	0.58	0.58	0.70	0.49	0.41	0.50
	0.1 mm	-	-	-	0.10	0.10	0.16	0.09	0.07	0.09
Tremolite-asbestos	2.0 mm	-	0.98	0.98	0.99	0.99	0.96	0.96	0.97	0.96
	1.0 mm	-	0.78	0.77	0.90	0.90	0.79	0.70	0.71	0.75
	0.5 mm	-	0.39	0.38	0.51	0.51	0.54	0.35	0.34	0.47
	0.1 mm	-	0.07	0.07	0.10	0.10	0.15	0.07	0.06	0.12
Chrysotile	2.0 mm	-	-	-	-	-	-	1.03	1.02	1.13
	1.0 mm	-	-	-	-	-	-	0.64	0.64	0.75
	0.5 mm	-	-	-	-	-	-	0.29	0.30	0.36
	0.1 mm	-	-	-	-	-	-	0.05	0.05	0.07
Anthophyllite-asbestos	2.0 mm	-	-	-	1.00	1.00	1.00	1.00	1.00	1.00
	1.0 mm	-	-	-	0.91	0.91	0.79	0.73	0.74	0.74
	0.5 mm	-	-	-	0.55	0.55	0.55	0.39	0.38	0.43
	0.1 mm	-	-	-	0.10	0.10	0.15	0.08	0.07	0.09
Actinolite-asbestos	2.0 mm	-	1.00	1.00	1.00	1.00	0.96	0.98	0.99	0.96
	1.0 mm	-	0.82	0.82	0.92	0.92	0.81	0.76	0.76	0.79
	0.5 mm	-	0.42	0.42	0.56	0.55	0.55	0.39	0.38	0.48
	0.1 mm	-	0.07	0.07	0.10	0.10	0.16	0.07	0.07	0.12

Tab. 3 - k-ratios calculated at 15 keV for bundle of fibres of square section of different thickness.

and Health Issues 67, 55-88.

Hawthorne F.C. and Oberti R., 2007b. Amphiboles: Crystal chemistry. Amphiboles: Crystal Chemistry, Occurrence, and Health Issues 67, 1-54.

Hawthorne F.C., Oberti R., Harlow G.E., Maresch W.V., Martin R.F., Schumacher J.C., Welch M.D., 2012. Nomenclature of the amphibole supergroup. American Mineralogist 97, 2031-2048.

Haynes W.M. (Ed.), 2015. CRC Handbook of Chemistry and Physics, 96th Edition. CRC Press, Boca Raton, FL, USA.

Jablonski A., Salvat F., Powell C.J., 2010. NIST electron elastic-scattering cross-section database. National Institute of Standards and Technology, Gaithersburg, MD.

Joy D.C. and Luo S., 1989. An empirical stopping power relationship for low-energy electrons. Scanning 11, 176-180.

Merlet C., Llovet X., 2011. New measurements of the surface ionization for quantitative electron probe microanalysis. X-Ray Spectrometry 40, 47-54.

Merlet C., Llovet X., 2012. Uncertainty and capability of quantitative EPMA at low voltage - A review. Emas 2011: 12th European Workshop on Modern Developments in Microbeam Analysis, 32.

Moro D., Ulian G., Valdrè G., 2015. Single molecule investigation of glycine-chlorite interaction by cross-correlated scanning probe microscopy and quantum mechanics simulations. Langmuir : the ACS journal of surfaces and colloids 31, 4453-63.

Moro D., Valdrè G., 2016. Effect of shape and thickness of asbestos bundles and fibres on EDS microanalysis: a Monte Carlo simulation. IOP Conference Series: Materials Science and Engineering 109, 012011.

Myklebust R., Newbury D., Yakowitz H., 1976. NBS Monte Carlo electron trajectory calculation program. In: Heinrich K., Yakowitz H., and Newbury D. (Eds), NBS Special Publication, 460, 105. National Bureau of Standards, Washington, DC.

Paoletti L., Bruni B.M., Arrizza L., Mazziotti-Tagliani S., Pacella A., 2008. A micro-analytical SEM-EDS method applied to the quantitative chemical compositions of fibrous

amphiboles. Periodico Di Mineralogia 77, 63-73.

Paoletti L., Bruni B.M., Gianfagna A., Mazziotti-Tagliani S., Pacella A., 2011. Quantitative energy dispersive x-ray analysis of submicrometric particles using a scanning electron microscope. Microscopy and Microanalysis 17, 710-717.

Ritchie N.W.M., 2009. Spectrum simulation in DTSA-II. Microscopy and Microanalysis, 15, 454-468.

Ritchie N.W.M., 2010. Using DTSA-II to simulate and interpret energy dispersive spectra from particles. Microscopy and Microanalysis 16, 248-258.

Salvat F., Llovet X., Fernandez-Varea J.M., Sempau J., 2006. Monte Carlo simulation in electron probe microanalysis. Comparison of different simulation algorithms. Microchimica Acta 155, 67-74.

Small J.A., 2002. The analysis of particles at low accelerating voltages (<= 10 kV. with energy dispersive x-ray spectroscopy (EDS). Journal of Research of the National Institute of Standards and Technology 107, 555-566.

Valdrè G., Botton G.A., Brown L.M., 1999. High spatial resolution peels characterization of FeAl nanograins prepared by mechanical alloying. Acta Materialia 47, 2303-2311.

Valdrè G., Moro D., Ulian G., 2018. Monte Carlo simulation of the effect of shape and thickness on SEM-EDS microanalysis of asbestos fibres and bundles: the case of anthophyllite, tremolite and actinolite. IOP Conference Series: Materials Science and Engineering 304, 012019.

Wiewiora A., 1990. Crystallochemical Classifications of Phyllosilicates Based on the Unified System of Projection of Chemical-Composition.3. The Serpentine-Kaolin Group. Clay Minerals 25, 93-98.

Yao S.D., Della Ventura G., Petibois C., 2010. Analytical characterization of cell-asbestos fiber interactions in lung pathogenesis. Analytical and Bioanalytical Chemistry 397, 2079-2089.